Commun. Comput. Phys.
doi: 10.4208/cicp.040809.231109a

Vol. **8**, No. 1, pp. 185-210
July 2010

Collisional-Radiative Calculations of Optically Thin and Thick Plasmas Using the Computational Package ABAKO/RAPCAL

R. Rodriguez[1,2,*], R. Florido[1,2], J. M. Gil[1,2], J. G. Rubiano[1,2], D. Suarez[1], P. Martel[1,2], E. Minguez[2] and R. C. Mancini[3]

[1] *Physics Department, University of Las Palmas de Gran Canaria, 35017, Spain.*
[2] *Nuclear Fusion Institute-Denim, Polytechnic University of Madrid, 28006, Madrid, Spain.*
[3] *Department of Physics, University of Nevada, Reno, NV 89557, USA.*

Received 4 August 2009; Accepted (in revised version) 23 November 2009

Communicated by Zhihong Lin

Available online 12 February 2010

Abstract. Non-local thermodynamic equilibrium (NLTE) conditions are universal in laboratory and astrophysical plasmas and, for this reason, the theory of NLTE plasmas is nowadays a very active subject. The populations of atomic levels and radiative properties are essential magnitudes in the study of these plasmas and the calculation of those properties relies on the so-called collisional-radiative (CR) models. However, the complexity of these models has led to the development of numerous collisional-radiative codes and this is a current research topic in plasmas. In this work is presented a versatile computational package, named ABAKO/RAPCAL, to calculate the populations of atomic levels and radiative properties of optically thin and thick, low-to-high Z, NLTE plasmas. ABAKO/RAPCAL combines a set of analytical approximations which yield substantial savings in computing running time, still comparing well with more elaborated codes and experimental data. In order to show the capabilities of the code and the accuracy of its results, calculations of several relevant plasma magnitudes for various plasma situations are shown and compared.

PACS: 52.25Dg, 52.25Os

Key words: Collisional-radiative model, optically thin and thick NLTE plasmas.

*Corresponding author. *Email addresses:* rrodriguez@dfis.ulpgc.es (R. Rodriguez), rflorido@dfis.ulpgc.es (R. Florido), jmgil@dfis.ulpgc.es (J. M. Gil)

1 Introduction

In many research areas on plasmas and their applications such as astrophysics, X-ray laser development, inertial and magnetic confinement fusion or EUV lithography, the accurate calculation of the populations of atomic levels and radiative properties existing in the plasma is required, since they are involved, for example, in hydrodynamic simulations or spectroscopic diagnostics.

At high densities, when the plasma can be considered under local thermodynamic equilibrium (LTE) conditions the populations are calculated by means of the equations of Saha-Boltzmann. On the other hand, in the low density regime, coronal equilibrium (CE) can be assumed and, therefore, these quantities are evaluated using the CE equations. However, these limit situations are exceptions and non-LTE (NLTE) conditions are universal in laboratory and astrophysical plasmas and, for this reason, the theory of NLTE plasmas is nowadays a very active subject. In NLTE, the problem shows great complexity because there is not a priori expression for the occupation probabilities of bound states and one must find the statistical distribution of the ionic levels using a collisional-radiative (CR) model. This implies solving a set of rate equations with coupling of atomic configurations, free electrons and photons. Taking into account that for accurate simulations of the level populations and radiative properties it is essential to include as many levels as possible, the resolution of the resulting large linear equation system becomes sometimes unmanageable and approximations must be made. This fact has led to the development of numerous CR codes [1–10] since the early proposals described in [11,12].

The complexity of the CR models is mainly due to three factors. The first one is the atomic model chosen, which is still the focus of much attention and numerous discussions. The most detailed level of information that can be used in the determination of the population distributions is usually referred detailed-level-accounting (DLA) approach, in which each atomic level is explicitly included and the resolution of a level-by-level kinetic model is required. This approach is considered practical for elements with a low to medium atomic number ($Z < 30$) [13]. As the atomic number increases, the amount of atomic data involved rises considerably and the DLA approach becomes impractical and sometimes unnecessary [14]. Thus, for high-Z elements, a configuration-by-configuration kinetic model, i.e. a detailed-configuration-accounting (DCA) model, is the standard approach. In the literature there are statistical methods to reduce the level of atomic description which imply grouping of levels into configurations (resulting a DCA model) [15] or superconfigurations (SC) [16]. These methods have shown to be very efficient when they are combined with unresolved transition array (UTA/SOSA) [17, 18] and/or supertransition array (STA) [19] formalisms. In these approaches both the amount of atomic data and the number of rate equations are noticeably reduced due to the configuration or superconfiguration average. However, these models based on averages may lack the accuracy to describe isolated levels or transitions. A possible improvement lies in the definition of effective temperatures inside each statistical group (configuration or superconfiguration), where the detailed level population inside each

group is obtained from the group population and the effective temperature [7]. Another alternative relies on the hybrid models that mix detailed and average descriptions [13,20] or the reduced DCA model [21], which, however, can be considered an area still under development. Other models try to optimize the speed of calculation, although that implies a certain loss of accuracy, because, for example, they are going to be used to perform in-line hydro-simulations, such as those developed in the context of an average atom.

The second difficulty in the CR models is related to the expressions employed for the rate coefficients of the atomic processes included. In principle, they should be obtained by means of quantum mechanical calculations. However, any kinetic calculation implies a massive evaluation of rate coefficients, which prevents its application. On the other hand, in the literature there are available analytical expressions for the rate coefficients or cross sections of the most relevant atomic processes, although no one of them stands out for its high accuracy. However, due to the complexity of the problem considered, it is necessary to reach a compromise between accuracy and computational viability.

Finally, there is the problem of the radiative transfer. For optically thick plasmas the radiative transfer equation is coupled to the rate equations in the CR model. The radiation transport shows a considerable relevance, for instance, in the study of planetary and stellar atmospheres and also in the population balance and spectral properties of laser generated dense plasmas. However, the exact resolution of the radiative transfer equation for each radiative transition in the plasma involves a huge computational cost. Furthermore, due to the coupling with the rate equations, the calculation requires an iterative procedure until the convergence is achieved. For this reason, we can find many different approaches and numerical techniques for dealing with the radiative transport under NLTE conditions [22–26]. There are also methods, based on the escape factor formalism, that avoid the explicit solution of the radiative transfer equation and can be applied to homogeneous [27–29] or non-homogeneous plasmas [30–32].

Thereby, according to the above explained, there are many sources of discrepancies among the different developed CR models. Obviously, the ability to reproduce experimental data is the most valuable test for any CR model, but clean experiments are very difficult to perform and there exist only a few measurements that could be used as benchmark cases for the validation of computational codes. The NLTE kinetics workshops [33–35], which have focused on comparisons for specific cases among CR codes developed by diverse research groups, try to make up for this lack of experimental data. These meetings have contributed to identify regimes of plasma conditions where population kinetics looks predictable, as it happens near closed shells, however the general rule for the most of the cases was the disagreement between codes. This demonstrates that none of the available models can be considered as the ultimate solution to the problem of the population kinetics, but rather represent complementary ideas and choosing one or the other will depend on the situation under review. In summary, further investigation into population kinetics of NLTE plasmas is necessary and any progress for providing a better understanding of the underlying physics will be welcomed.

Thus, in this work we present the ABAKO/RAPCAL computational package, a CR

code to determine the population distribution of atomic levels and radiative properties of steady-state optically thin and thick plasmas, which is the result of coupling ABAKO [36, 37] and RAPCAL [38] codes. During its development, a special care was taken to achieve an optimal compromise between accuracy and computational cost. Hence, the code combines a set of simple analytical models which yield substantial savings of computer resources, still providing good comparisons with more elaborate codes and experimental data. It incorporates an internal atomic model that provides atomic data in the DCA approach making use of a parametric potential, although working with an external source of atomic data is also available. Analytical expressions are employed to compute the rate coefficients of the atomic processes involved in the kinetics and the opacity effects are taken into account using a model based on the a escape factor formalism. These features make ABAKO/RAPCAL a versatile CR model which can be applied to low-to-high Z ions for a wide range of laboratory plasma conditions: coronal, LTE or NLTE, optically thin or thick plasmas. Next section is devoted to describe the main features of the code. In Section 3 are presented and compared calculations of several relevant plasma magnitudes for various plasma situations, in order to show the capabilities of the code and its accuracy. Finally, in Section 4 are exposed main conclusions and remarks.

2 ABAKO/RAPCAL description

The ABAKO/RAPCAL code is composed by three modules. This section is devoted to their explanation as well as to comment some computational aspects related to the resolution of the linear system of rate equations. A flowchart of the code is plotted in Fig. 1.

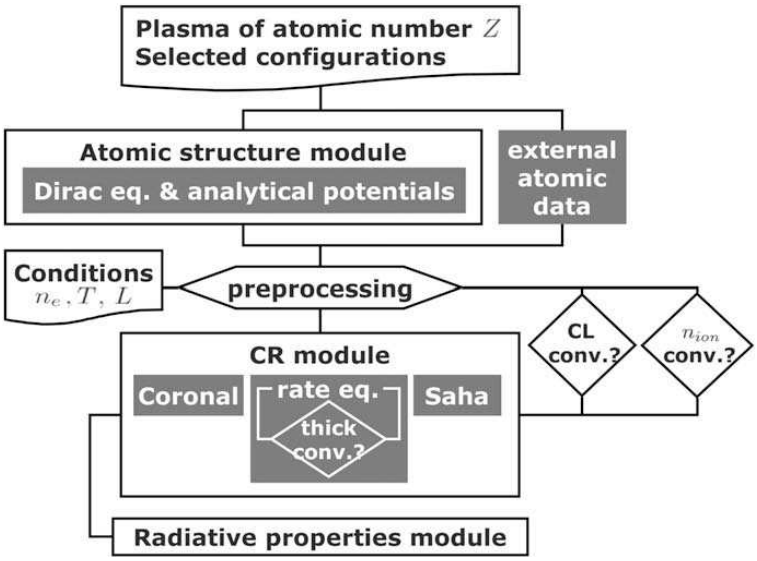

Figure 1: ABAKO/RAPCAL flowchart.

2.1 Atomic module

ABAKO/RAPCAL has a built-in model to obtain all the atomic data required for kinetic calculations. The model follows a relativistic DCA approach within the central field approximation. For each relativistic configuration, the Dirac equation is solved using as effective potential an analytical one which can model both isolated situations [39,40] and ions immersed into weakly [41] and strongly coupled plasmas [42]. In spite of its simplicity, this atomic model is able to provide accurate results for magnitudes such as the average ionization and ion population and, therefore, it is often used as a first step in more elaborate calculations in order to optimize them. For example, it has been used in obtaining the maps of the thermodynamic regimes and average ionization of carbon [43] and aluminum [38] plasmas in terms of the electron temperature and density. However, for less average plasma magnitudes such as the atomic level populations or radiative properties it is required a better atomic description. ABAKO/RAPCAL has been also designed to work with external atomic data obtained either from atomic data tables or codes. The current external atomic source is the FAC code [44]. FAC is designed to provide atomic data in DLA approach, but it can also works in a DCA mode by means of configuration averages of detailed levels. The energies of the levels of an ion are obtained by diagonalizing the relativistic Hamiltonian. The basis states which are usually referred as configuration state functions are built as anti-symmetric sums of products of one-electron Dirac spinors. In coupling the angular momenta the standard *jj*-coupling scheme is followed. Finally, the approximate atomic wave functions are evaluated mixing the basis states with the same symmetry with the mixing coefficients obtained from diagonalizing the total Hamiltonian. A simple computational program has been written to automatically convert the FAC output files into properly formatted ABAKO/RAPCAL input ones.

As the plasma density increases, screening effects due to neighboring electrons and ions begin to modify the energy levels while degeneracy begins to raise the energy of the free electrons. The resulting change in the ionization potentials of bound states and level occupancy numbers leads to the phenomenon of pressure ionization. In spite of the well-known critical importance of pressure ionization to calculate the ionic abundances and level populations, great difficulties are still found to model it properly and the most of the existing CR models and codes take into account the plasma effects in a very approximate way. The phenomenon is often described only in terms of a lowering of the ionization potential or continuum-lowering (CL) and this is the procedure that we follow in ABAKO/RAPCAL too. Thus, for dense plasmas, the isolated ionization potential I_ζ is lowered a quantity ΔI_ζ to obtain a non-isolated value $I'_\zeta = I_\zeta - \Delta I_\zeta$. To calculate the correction ΔI_ζ we apply the formulation due to Stewart and Pyatt [45], but using the particular proposal given in [46],

$$\Delta I_\zeta = \frac{3}{2}\frac{I_H a_0}{R_\zeta}(\zeta+1)\left\{\left[1+\left(\frac{D}{R_\zeta}\right)^3\right]^{2/3}-\left(\frac{D}{R_\zeta}\right)^2\right\}. \tag{2.1}$$

Here I_H is the Rydberg constant, a_0 is the Bohr radius, $R_\zeta = [3(\zeta+1)/(4\pi n_e)]^{1/3}$ is the ion-sphere radius assuming the plasma composed of ions with charge ζ only, the Debye radius is $D = \left[4\pi(\bar{Z}+\overline{Z^2})n_{ion}/T_e\right]^{-1/2}$, $a = 1/D$, $\bar{Z}$ is the plasma average ionization, $\overline{Z^2}$ is the second order moment of the population distribution, n_{ion} is the total ion density and T_e is the electron temperature (assuming ion-electron termalization). Note that when the CL correction is applied the kinetics rate equations must be solved iteratively, since the atomic data depend on ionization balance by means of $\bar{Z}$ and $\overline{Z^2}$.

Finally, the issue of which set of electronic configurations must be included in a particular kinetic calculation must be addressed. Both, the level populations and radiative properties depend strongly on the atomic configurations included in the calculations, however, it is still an open question which is the most suitable election of them [14,20,47]. In this respect, the overall analysis of the large number of cases studied during the ABAKO/RAPCAL development has led us to consider a complete enough set of configurations which allows us to obtain reasonable estimates of the ionization balance. This set of selected configurations has been shown to be robust for atomic kinetic modeling, since the addition of new configurations produced hardly appreciable changes in the population distributions.

2.2 Collisional-radiative module

This module is basically the ABAKO code. Following the standard NLTE modeling approach, where an account of the existing atomic states is made and the microscopic (radiative and collisional) processes connecting these states are identified, a rate equation system describing the population density of the atomic states is built and solved, giving the population distribution. Therefore, to find the level population distribution the following system of rate equations is solved,

$$\frac{\partial N_{\zeta i}(\mathbf{r},t)}{\partial t} + \mathbf{v}\cdot\nabla N_{\zeta i}(\mathbf{r},t) = \sum_{\zeta' j} N_{\zeta' j}\mathbb{R}^{+}_{\zeta' j\to\zeta i} - \sum_{\zeta' j} N_{\zeta i}\mathbb{R}^{-}_{\zeta i\to\zeta' j}, \tag{2.2}$$

where $N_{\zeta i}$ is the population density of the atomic level ζi. The terms $\mathbb{R}^{+}_{\zeta' j\to\zeta i}$ and $\mathbb{R}^{-}_{\zeta' j\to\zeta i}$ take into account all the atomic processes which contribute to populate and depopulate the state ζi, respectively. In this paper no radiation-driven processes are explicitly considered. Also, a Maxwellian energy distribution with a characteristic temperature T_e for free electrons will be assumed.

Two complementary equations which have to be satisfied together with (2.2) are, first, the requirement that the sum of all the partial densities equals the total ion density,

$$\sum_{\zeta=0}^{Z}\sum_{i=0}^{M_\zeta-1} N_{\zeta i} = N_{ion}, \tag{2.3}$$

and, second, the charge neutrality condition in the plasma,

$$\sum_{\zeta=0}^{Z}\sum_{i=0}^{M_\zeta-1}\zeta N_{\zeta i}=n_e, \tag{2.4}$$

where M_ζ is the total number of levels for the charge state ζ.

Furthermore, if the plasma is optically thick, the set of the rate equations must be solved together with the radiative transfer equation,

$$\frac{1}{c}\frac{\partial I(\mathbf{r},t,\nu,\mathbf{e})}{\partial t}+\mathbf{e}\cdot\nabla I(\mathbf{r},t,\nu,\mathbf{e})=-\kappa(\mathbf{r},t,\nu)\,I(\mathbf{r},t,\nu,\mathbf{e})+j(\mathbf{r},t,\nu), \tag{2.5}$$

where I is the specific intensity, ν the photon frequency, $\mathbf{e}$ a unitary vector in the direction of the radiation propagation, and κ and j the absorption and emission coefficients, respectively, which couple the radiative equation with the rate equations.

In ABAKO is assumed in the rate equations static ions and stationary situations which yields that the left member in (2.2) equals zero. The processes included in the CR model are the following: collisional ionization [48] and three-body recombination, spontaneous decay, collisional excitation [49] and deexcitation, radiative recombination [50], electron capture and autoionization. We have added between brackets the references wherefrom their approximated analytical rates coefficients have been acquired. The rates of the inverse processes are obtained through the detailed balance principle. It is worth pointing out that the autoionizing states are included explicitly. It has been proved that their contribution is critical in the determination of the ionization balance. The cross section of the autoionization process is evaluated using detailed balance principle from the electron capture cross section. This one is obtained from the collisional excitation cross section using a known approximation [51]. Only those atomic processes whose rates are independent of the radiation field intensity are explicitly considered in the CR model.

With respect to the radiative transfer equation, in ABAKO is assumed stationary conditions. Therefore, the first sum in the left hand of (2.5) equals zero. In the current version of ABAKO only bound-bound opacity effects are taken into account. These ones are included in an approximate way by means of the escape factor formalism which avoids the explicit solution of the radiative transfer equation. For a given line transition $\zeta i\leftrightarrow\zeta j$, the escape factor Λ_{ji} is introduced as an alternative way of writing the net rate of line emission. The escape factors enter in the calculations in two ways. First, in the atomic physics calculations of excited-state populations. As a result there is an effective reduction in the Einstein spontaneous emission coefficient $\mathcal{A}_{\zeta j\to\zeta i}$, which is written as $\Lambda_{ji}\mathcal{A}_{\zeta j\to\zeta i}$. Second, they appear in the determination of the total emergent line intensity. This modification circumvents the need to perform a simultaneous calculation of radiation transport and atomic physics. To compute the escape factors we have adopted the technique described in [52]. Thus, assuming a uniform distribution of emitting atoms and isotropic emission, for the three basic geometries—plane, cylindrical and spherical—the escape factor Λ_{ji} is

written as

$$\Lambda_{ji}=\int_0^\infty \phi_{ij}(\nu)\frac{1}{\tau_{ij}(\nu)}F\left[\tau_{ij}(\nu)\right]d\nu. \tag{2.6}$$

Here $\phi_{ij}(\nu)$ is the line profile. By default ABAKO considers a Voigt profile accounting for natural, collisional and Doppler broadenings. Stark broadening can be also included as an extra Lorentzian width using the approximate semiempirical formula given in [53]. Other line profile shapes can be used in the escape factors calculation if they are externally provided. $\tau_{ij}(\nu)=\kappa_{\zeta i\to\zeta j}(\nu)L$ is the optical depth, where in turn $\kappa_{\zeta i\to\zeta j}(\nu)$ is the line absorption coefficient and L denotes the characteristic plasma dimension, i.e. slab width, cylinder or sphere radius. Finally, $F\left[\tau_{ij}\right]$ is a functional of the optical depth whose particular form depends on the considered geometry. Thus, for the slab it is obtained [54]

$$F(\tau)=\frac{1}{2}-E_3(\tau), \tag{2.7}$$

where $E_3(\tau)$ is the third-order exponential integral, for the spherical case it takes the form [52]

$$F(\tau)=\frac{3}{4}\left\{1-\frac{1}{\tau^2}\left[\frac{1}{2}-\left(\tau+\frac{1}{2}\right)e^{-2\tau}\right]\right\}, \tag{2.8}$$

and for the cylindrical geometry $F(\tau)$ is computed by interpolation over a numerically defined function as described in [55]. Unlike other widely used methods for evaluating the escape factor, such as [30–32], the formalism used in ABAKO has the advantage that details about geometry are treated in an exact way. Moreover, according to (2.6), the last integral that needs to be solved is a frequency integral over the line profile. This fact facilitates the use of other line profile functions, such as those provided by elaborate Stark calculations, for the calculation of the escape factor. Thereby, it is no longer dependent on rigid parametrizations of the frequency integral, which, although fast from a computational point of view, are only available for the typical Lorentzian, Gaussian and Voigt profiles, as it happens in [30–32].

On the other hand, for each line transition, the escape factor depends implicitly on the populations of the lower, $N_{\zeta i}$, and upper level, $N_{\zeta j}$, since, according to (2.6), they are required to compute the absorption coefficient $\kappa_{\zeta i\to\zeta j}(\nu)$. Hence, in the case of optically thick plasmas, the system of rate equations must be solved iteratively until convergence is achieved within a prescribed tolerance.

Furthermore, ABAKO incorporates a new technique for the line-photon transport relied on the definition of zone-to-zone radiative coupling coefficients. As a remarkable attribute it can be applied to non-uniform planar media, i.e. with spatially varying electron temperature and density, wherein other proposals developed within the same framework seem not to be appropriate. We consider a plasma with planar geometry divided along Z axis in N_C homogeneous slabs, each of them characterized by an electron density N_e^c and

temperature T_e^c, with $c=1,\cdots,N_C$. In the cell a the escape factor can be written as

$$\Lambda_{ji}^q = C_{ji}^q + \sum_{\substack{p=1 \\ p\neq q}}^{N_C} \frac{S_{ij}^p}{S_{ij}^q} C_{ji}^{pq}, \tag{2.9}$$

where the first term gives the probability that a photon emitted in the cell a escapes from it without being absorbed and S_{ij}^p denotes the monochromatic source function in the cell q. The sum can be interpreted as the probability that the photon is absorbed in any of the remaining cells. Following the ideas described in [52] and [31], we have found the following expressions for the radiative coupling coefficients for a plane-parallel medium

$$C_{ij}^q = \int_0^\infty d\nu \phi_{ij}^q(\nu) \frac{1}{\Delta\tau_{ij}^q} F\left(\Delta\tau_{ij}^q\right), \tag{2.10}$$

$$\begin{aligned} C_{ij}^{pq} = \frac{1}{2}\int_0^\infty d\nu \phi_{ij}^q(\nu) \frac{1}{\Delta\tau_{ij}^q} \Big[& F\left(\tau_{ij}^{pq}+\Delta\tau_{ij}^q\right) - F\left(\tau_{ij}^{pq}\right) \\ & - F\left(\tau_{ij}^{pq}+\Delta\tau_{ij}^q+\Delta\tau_{ij}^p\right) + F\left(\tau_{ij}^{pq}+\Delta\tau_{ij}^p\right) \Big], \end{aligned} \tag{2.11}$$

with $F(\tau)=\frac{1}{2}-E_3(\tau)$, τ_a is the optical depth of cell a and τ_{ac} is the optical depth between cells a and c. In the above equations the details of geometry are exactly solved. In addition, as the frequency integration is approached as the last step in the procedure, a specification of the profile function before the geometry-dependent integrals is no longer needed and the consideration of more sophisticated profile functions (i.e. to include Stark effect) becomes feasible. We have found (2.10) and (2.11) under some approximations. It was assumed that complete frequency redistribution holds, so absorption and emission profiles becomes equal for each line in a given cell. We also consider that there is no overlapping between different lines, and, therefore, the source function in each cell can be approximated to the monochromatic one, and continuum-radiation effects are not included.

2.3 Radiative properties module

The third module is the RAPCAL code [38], which is devoted to determine plasma radiative properties, such as spectrally-resolved and mean emissivity and opacity, specific intensity, source function, transmission and radiative power losses. The bound-bound spectrum includes all the allowed transitions in the dipole approximation between all the detailed atomic levels or configurations considered. Line profiles incorporate Doppler, natural and electron-impact widths. For the latter a semiempirical formula is used [53]. Complete redistribution is assumed, so the same profile is used for the emission and the absorption processes. For the bound-free spectrum, it evaluates the cross section in the distorted wave approximation if we employ atomic data from FAC or the semiclassical expression of Kramers [50] if we employ the atomic module implemented in

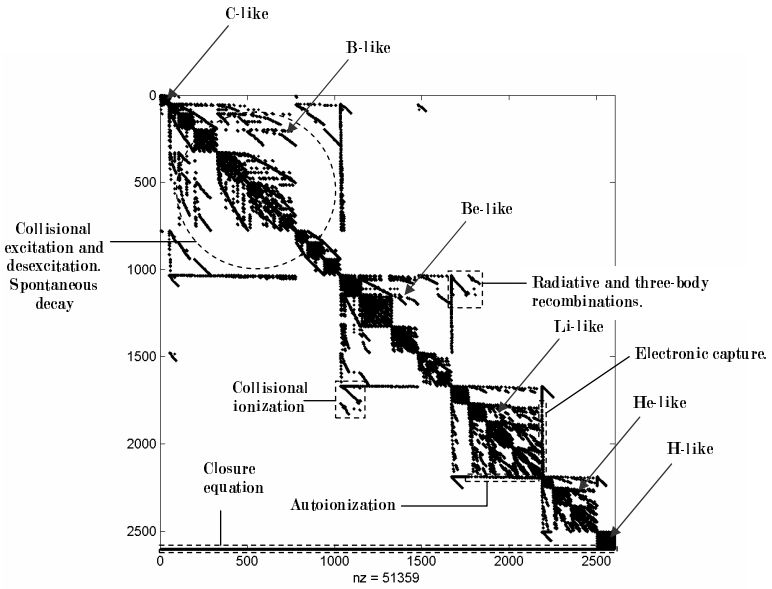

Figure 2: Standard CR matrix in an optically thin calculation.

ABAKO/RAPCAL. Finally, for the free-free spectrum, the semiclassical expression of Kramers [56] is always used. Full details about RAPCAL along with a collection of representative results—including spectrally resolved and mean opacities and emissivities, radiative power losses and transmission spectrum for plasmas of several atomic numbers for LTE and NLTE conditions—can be consulted in [38].

2.4 Resolution of the linear system of rate equations

When the electron density is taken as an input parameter characterizing the population kinetics problem, then the set of rate equations constitutes a linear system of M equations for the level populations, where M denotes the total number of levels included in the CR model. Hence the size of the CR matrix scales like M^2. However, modeling population kinetics the atomic processes usually connect only levels that belong either to the same charge state or to adjacent ones and this means that the CR matrix is sparse as it is shown, as an example, in Fig. 2. In this example, the number of levels is 2605 and, therefore, the number of matrix elements is 2605^2. However, from the figure it is observed that the amount of non-zero elements (51359) is lower than the 1% of the total. When we are dealing with non-homogenous optically thick plasmas, the structure of Fig. 2 is repeated as many times as the number of cells considered and there are non-zero matrix elements that connect different cells due to the radiative coupling coefficients, see Fig. 3. In this case, the percentage of non-zero elements is even lower. Therefore, in order to keep memory requirements to a minimum, ABAKO/RAPCAL uses sparse techniques to store and operate on only the nonzero CR matrix elements.

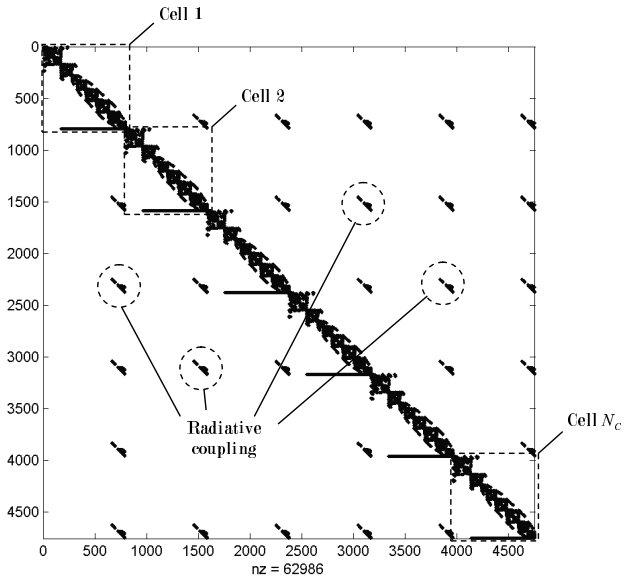

Figure 3: Standard CR matrix in an optically thick non-homogeneous calculation.

Another issue to consider is the method chosen for the solution of the rate equations solver. Solvers can be broadly classified into two categories, direct and iterative. Using standard linear algebra techniques, the direct solvers compute a solution which is guaranteed to be as accurate as the problem definition. The amount of time required to obtain a solution by such algorithms typically scales like M^3. In a population kinetics problem the number of levels can easily reach the order of 10^4-10^5, so for such large systems of equations the direct methods lead to prohibitively long run times. On the other hand, the iterative methods start with an initial guess to the solution and proceed to calculate solution vectors that approach the exact solution with each iteration, being the process ended when a given convergence criterion is satisfied. For the kind of problems that we are interested in the iterative methods yield an approximation to the solution significantly faster than a direct method. Furthermore, iterative techniques typically require less memory than direct ones and hence can be the only means of solution of the large CR system of equations. In its current version, ABAKO/RAPCAL uses the generalized minimum residual (GMRES) or preferably the bi-conjugate gradient (BCG) iterative method implemented in either the SPARSKIT [57] or CXML [58] numerical packages. Among the existing iterative algorithms, BCG proved to be very efficient to solve the system of rate equations according to the numerical tests that we performed. These consisted of comparisons of the populations obtained by the BCG solver with those provided by more accurate direct solvers. Since ABAKO/RAPCAL intends to be a flexible and portable package, tests were run on simple Windows XP PC's with Intel Pentium IV 3 GHz or Dual-Core 1.7 GHz and 1 Gb RAM memory. The results are listed in Table 1. For a wide range of plasma conditions, the agreement between direct and iterative methods was

very good. It is worth pointing out that the number of needed iterations to achieve convergence depends on the initial guess. Thus, in order to initialize the iterative solver with a good initial guess and accelerates the convergence, ABAKO/RAPCAL uses as initial population distribution the solution provided by either the corona model or the Saha-Boltzmann equations depending on whether the electron density of the case analyzed is closer to the regime of low or high-density, respectively.

Table 1: Comparison between direct and iterative methods to perform the CR matrix inversion. Calculations were done for an aluminum plasma.

Number of levels	Computation time (s)	
	Direct method	Iterative method
1000	1	<1
1500	3	<1
2000	4	1
2500	8	1
3000	14	2
3500	16	3
4000	33	4
5000	66	6
6000	84	10
7000	261	13
8000	1451	18

We have also developed a parallelized version of the first and second modules of the code for homogeneous plasmas making use of the Message Passing Interface (MPI) [59]. We have developed a master-slave approach in order to improve the execution time. The code has been compiled and tested with open MPI, LAM/MPI (Local Area Multicomputer) and MPICH2 (MPI Chameleon) libraries [60, 61]. In order to assure compatibility, any of the MPI-2 extensions were used. In our master-slave approach, the master (main process) sends a *New Task* and *Task Type* message to all the slaves, setting them into a *Task Status*. The tasks supported are: receive configuration options; receive atomic data; start atomic process calculation and generate rate equations, and kill slave. The last task is only used at the end of the execution. That approach give as an easy maintenance of the code, allowing us to add other parallelized routines in the future.

The parallelization features are used both in the calculation of the atomic processes and in the generation of the rate equations. The master process assigns an equal number of atomic levels to each slave. Then, it sends the task start atomic process calculation and generate rate equations. Each slave starts to calculate its assigned atomic processes and to generate the corresponding rate equations.

In Table 2 are listed the execution time, in seconds, for CR calculations of low, medium and high-Z optically thin plasmas as a function of the number of processes considered. Along with the name of the chemical element it has been added, in brackets, the number of levels, and, therefore, the number of rate equations, considered. The calculations were

Table 2: Execution time, in seconds, for several plasmas as a function of the number of processes considered. In brackets we have added the number of levels and the percentage of execution time.

Process	Carbon (2717)	Argon (4592)	Iron (8150)	Iron (16302)	Gold(45168)
1	8.88 (100 %)	24.69 (100 %)	47.89 (100 %)	173.03 (100 %)	13396 (100 %)
2	7.86 (88.5 %)	18.28 (74.0 %)	40.53 (84.6 %)	134.08 (77.5 %)	10207 (76.2 %)
3	8.30 (93.5 %)	17.39 (70.4 %)	31.31 (65.4 %)	99.34 (57.4 %)	6644 (49.6 %)
4	7.90 (89.0 %)	17.72 (71.8 %)	29.88 (62.4 %)	88.23 (51.0 %)	5261 (39.3 %)

carried out using an Intel QuadCore Q6600 2.4 Ghz and 2 Gb RAM. From the table we observe that, except for the carbon case, the execution time decreases as the number of processes grows. For the former, the execution time is almost the same or even higher when the number of processes rises. When there are few atomic levels, as it happens in the carbon case, the execution time is almost the same or even higher. It is due to the setting up and interprocess communication time. On the other hand, when the number of atomic levels is high the execution time tends to the inverse of the number of processes, as the theory establishes. Anyway, it is worth pointing out that even with as low as 5000 atomic levels the execution time is reduced significantly. Moreover, that reduction will be more important when the rate equations have to be calculated several times (because continuum lowering corrections are applied, or the electronic density is computed from the density of matter or ions, or we are modeling optically thick plasmas using the escape factor formalism).

Finally, a brief reflection about the solving of rate equations when the neutral ion stage is included in the calculations. The system of rate equations expressed in (2.2) is not linearly independent. Hence, when computing a solution to the steady-state case, a boundary condition is needed to provide sufficient information for determining a complete set of level populations. Usually the charge neutrality condition (2.4) is taken as boundary condition and used to replace one of the rows of the CR matrix and thus obtaining a non-trivial solution. When the neutral atom is not present in the calculations the charge neutrality results in a row with all non-zero elements and the iterative solver works fine. Nevertheless, when the neutral stage is included, since $\zeta = 0$ for the neutral, the charge neutrality condition introduces as many zero elements as atomic levels have been considered for modeling the neutral atom. Furthermore, taking into account that the neutral atom is the charge state having the largest number of bound electrons in a plasma of a given element, it will typically involve a large number of atomic levels, which in turn introduces by means of (2.4) the same large number of zero elements in the CR matrix. When the plasma conditions require to include the neutral atom in the kinetic calculations because its population is not negligible, for a certain number of cases, the use of the neutrality condition as boundary equation lead to an ill-conditioned—close to be singular—CR matrix, which causes the iterative method does not converge or it yields to an unreliable approximate solution. For this reason, ABAKO/RAPCAL uses the particle conservation (2.3) as boundary condition rather than the charge neutrality equation.

Thus, (2.3) introduces in the CR matrix a row full of ones. Then, in ABAKO the overall set of equations is divided by N_{ion} and the system is solved for the partial population densities $x_{\zeta i}=N_{\zeta i}/n_{ion}$. We have found that this procedure avoids convergence problems in order to invert the CR matrix and obtain the level population distribution.

3 Results

It is not our aim in this work to carry out an exhaustive study of plasma properties rather than to present some results and comparisons of several relevant plasma magnitudes for optically thin and thick situations that allow us to show the capabilities of the code and the accuracy of its results.

Table 3: Average ionization of the NLTE-4 carbon *test case*. DCA and DLA calculations are displayed in each case.

T_e (eV)	n_e (cm^{-3})	Colgan *et al.*		ABAKO/RAPCAL	
		DCA	DLA	DCA	DLA
3	10^{13}	1.486	1.730	1.605	1.619
	10^{15}	1.895	1.923	1.786	1.852
	10^{17}	1.948	1.952	1.917	1.913
	10^{19}	0.959	1.004	1.142	0.932
5	10^{13}	2.055	2.165	2.057	2.135
	10^{15}	2.592	2.514	2.309	2.276
	10^{17}	2.979	2.976	2.948	2.878
	10^{19}	2.104	2.076	2.182	2.084
7	10^{13}	2.729	2.887	2.722	2.873
	10^{15}	3.189	3.185	3.004	2.977
	10^{17}	3.718	3.729	3.529	3.545
	10^{19}	2.993	2.987	3.001	2.998
10	10^{13}	3.701	3.723	3.684	3.705
	10^{15}	3.856	3.862	3.747	3.745
	10^{17}	3.978	3.979	3.955	3.956
	10^{19}	3.785	3.786	3.776	3.787

3.1 Optically thin plasmas

To illustrate this case, we have chosen plasmas of low and medium-Z, carbon and krypton, respectively. In Table 3, we have listed the average ionization obtained for several electron temperature and densities chosen as test cases in the NLTE-4 Workshop [34]. The values obtained with ABAKO/RAPCAL are compared with those given by the Los Alamos National Laboratory code ATOMIC [62]. The calculations were performed both under DLA and DCA approaches. In ABAKO/RAPCAL for the DLA calculations were used data provided by FAC code including mixing of levels coming from the same

non-relativistic configuration, whereas for the DCA calculations were employed its own atomic module. From the table it is observed a general agreement between the results of both codes.

For the case of Kr plasmas, in Table 4 we present the cases considered and the average ionization obtained for those cases. The calculations were made using the atomic data obtained using the atomic module of ABAKO/RAPCAL. The results are compared with those reported by Chung *et al.* [63]. In that work, the calculations performed were very sophisticated. The atomic data were generated by the HULLAC suite of codes [3]. For atomic structure data HULLAC calculates the multiconfiguration, intermediate coupling energy eigenvalues of the fine structure levels, and configuration interaction is taken into account for energy levels calculations and oscillator strengths [64]. Autoionization rates [65] and photoionization cross sections were computed using the multiconfiguration wave functions and the collisional excitation and ionization were obtained in the distorted wave approximation [66]. A good agreement between our results and those given in [63] is found, which is a remarkable fact since, as it was stated before, their calculations are very complex. We can observe that for the two lowest densities and for all the temperatures considered, the plasma average ionization is independent of the density. This fact implies that in these cases the krypton plasma can be assumed under CE conditions.

Table 4: Average charge state of krypton ions. Our results are compared with those given by Chung *et al.*

n_e (cm^{-3})	10^{14}		10^{18}		10^{22}	
T_e (eV)	This work	Chung *et al.*	This work	Chung *et al.*	This work	Chung *et al.*
1000	25.33	25.48	25.36	25.56	26.69	27.46
1600	26.16	26.64	26.15	26.68	28.65	29.49
2000	26.86	27.82	26.87	27.86	30.16	30.81
2500	28.07	29.70	28.06	29.72	31.65	31.95
3000	30.48	31.24	30.48	31.24	32.51	32.61
3500	31.74	32.12	31.75	32.13	32.97	32.98
4000	32.46	32.65	32.47	32.65	33.22	33.21
4500	32.87	32.96	32.88	32.97	33.38	33.36
5000	33.12	33.17	33.13	33.18	33.49	33.47
6000	33.40	33.42	33.40	33.43	33.61	33.62
7000	33.57	33.58	33.57	33.58	33.71	33.72
8000	33.68	33.69	33.68	33.69	33.79	33.80
10000	33.86	33.84	33.86	33.84	33.93	33.92

We have also calculated the radiative power loss for low-electron-density krypton plasmas for a wide range of temperatures. Our calculations were performed using the atomic module of ABAKO/RAPCAL and the results are listed in Table 5. They are compared with those obtained using the analytical expression, valid for low density regime only, proposed by Fournier *et al.* [67]. This expression was fitted to total radiative cooling coefficients computed by them and validated with krypton cooling rates derived from

Table 5: Radiative power loss (ergs/s/cm^3) for low densities and several temperatures. Comparison between ABAKO/RAPCAL results and those obtained using the fit provided by Fournier *et al.*

n_e (cm^{-3})	10^{12}		10^{13}		10^{14}	
T_e (eV)	This work	Fournier *et al.*	This work	Fournier *et al.*	This work	Fournier *et al.*
10	5.600×10^5	2.381×10^5	5.599×10^7	2.382×10^7	3.573×10^9	2.359×10^9
20	3.220×10^5	1.387×10^5	3.217×10^7	1.387×10^7	1.416×10^9	1.387×10^9
50	3.124×10^4	3.467×10^4	3.124×10^6	3.467×10^6	3.123×10^8	3.467×10^8
100	3.522×10^4	7.154×10^4	3.522×10^6	7.154×10^6	3.522×10^8	7.154×10^8
200	9.155×10^4	1.011×10^5	9.155×10^6	1.011×10^7	9.155×10^8	1.011×10^9
500	1.949×10^4	6.331×10^4	1.949×10^6	6.331×10^6	1.949×10^8	6.331×10^8
1000	1.854×10^4	2.726×10^4	1.854×10^6	2.726×10^6	1.854×10^8	2.726×10^8

tokamak experiments. From the table, we can observe that both results are in general quite similar. Obviously, there are discrepancies but they are small and derive from the differences in the atomic models employed. In these low density situations, the CE can be assumed. Under this regime, the plasma average ionization and level populations are almost independent of the density and, therefore, the radiative cooling coefficient do not change. In Table 5, the results shown are obtained as the total radiative cooling coefficient multiplied by the electron and ion densities. Therefore, an increase of the electron density in one order of magnitude produces that the radiative power loss rises in two orders, see Table 5. However, we can observe for the highest density and the two lowest temperatures considered, that our results exhibit a different behavior. This fact implies that for these temperatures, the CE assumption is not accurate enough. Obviously, the calculation performed using the analytical fit do not present this discrepancy since it does not depend on the density.

3.2 Optically thick homogeneous plasmas

For this subsection we present two applications of ABAKO/RAPCAL for *K*-shell spectroscopic diagnostics of laser-produced optically thick plasmas. For the first one we have chosen an experimental study to measure the opacity and emissivity of bound-bound transitions in laser-shocked dense and hot aluminum plasma was carried out at the Laboratoire pour l'Utilisasion des Laseres Intenses (LULI) [68]. In the experiment the neodymium laser chain provided a 600 ps Gaussian pulse with a maximum energy of 80 J and a wavelength of 1053 nm. A 4ω beam was focused onto a structured target, the 100 μm focal spot yielded intensities as high as 2×10^{14} Wcm^{-2} irradiating the edge of a three-layered foil (CH/Al/CH). The plastic was entirely converted into plasma during the laser shot, thus ensuring the aluminum plasma confinement. The laser-target interaction gives rise to a nick instead of a crater and this was the key to guarantee a rigorous transversal observation of the ultra-dense plasma. In addition, this setup automatically produced a progressive spatial integration along the laser-target axis, the z axis, in the recorded film.

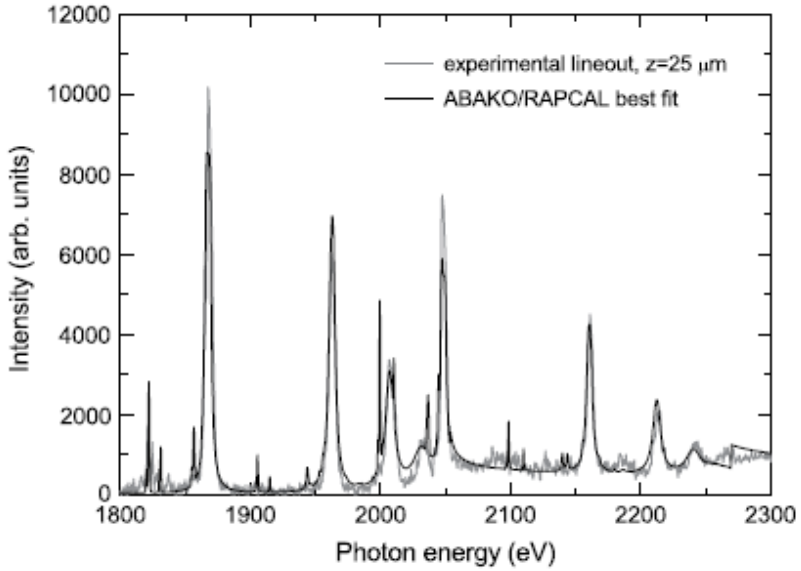

Figure 4: An example of ABAKO/RAPCAL best fit for an aluminum K-shell emission spectrum.

Although the plasma is non-homogeneous in the z axis, the transversality of the observation assures that the intensity corresponding to each lineout in the film comes from an homogeneous tegion of the plasma. The observed spectra includes the Lyα, Heβ, Heγ, Lyβ and Lyγ line emissions and their associated He- and Li-like satellites. Further details related to the experiment can be found in [68].

For this particular application, ABAKO/RAPCAL computed a database of emergent intensities in the photon energy range from 1700 to 2400 eV over a 20×20 grid of electron temperatures and densities in the domain of interest, i.e. 300-500 eV and 10^{21}-10^{23} cm^{-3}. For these calculations an optically 80-μm thick aluminum plasma was assumed, which matches with the thickness of the aluminum layer of the target for the case analyzed here. To satisfy the required accuracy in the atomic data, we calculated them using FAC. We employed a semiempirical formula for estimating Stark widths [53]. Natural, Stark and Doppler broadenings were taken into account in the context of Voigt line profiles. Complete redistribution was assumed and line overlapping considered. Finally, the extraction of the electron temperature and density for a given spectral lineout is performed by searching in the database the synthetic spectrum that yields the best fit to the data, in the sense of a least square minimization. An example is given in Fig. 4. As we can observe, there is, in general, a good agreement between the experimental spectrum and the theoretical simulation. For this lineout, the theoretical calculation gave an electron density of 1.198×10^{22} cm^{-3} and an electron temperature of 396 eV. A systematic application of this procedure to each of the lineouts in the recorded film results in a spatial profile of electron temperatures and densities.

The second example that we present is an analysis of the argon K-shell line and ra-

diative recombination emission from an argon-doped, deuterium-filled implosion core plasma, for the photon energy from 3500 eV to 4300 eV for electron temperature and density values relevant for the conditions achieved in OMEGA direct-drive implosion cores, i.e. 800-200 eV and 5×10^{23} to 5×10^{24} cm^{-3}, respectively. The main goal of the analysis is to study the relevance of the bound-free emission in modeling the argon spectrum in that photon energy range. Details of the experiment can be found in [69]. An ABAKO/RAPCAL model for argon was constructed that includes up to 4592 energy levels (1 fully-stripped, 100 H-like, 352 He-like, 519 Li-like, 644 Be-like, 1299 B-like and 1677 C-like Ar). Energy levels and radiative line transition rates were computed using the atomic structure code FAC including UTA and configuration interaction corrections. The calculations take into account all non-autoionizing and autoionizing states characterized by principal quantum numbers consistent with the CL. For the temperature and density conditions studied here this means that states with principal quantum number n up to 4 or 5 are typically considered in the calculation, including the effects of high-order satellites that overlap and blend with the parent line transition, thus affecting both the emissivity and opacity of the composite spectral feature. The emergent line intensity distribution is computed using an analytical integration of the radiation transport equation for the case of a uniform, spherical plasma source [70]. The intrinsic line shapes used to transport the line radiation through the plasma are detailed Stark-broadened line profiles. To this end, a database of line profiles was computed for line transitions arising from non-autoionizing as well as autoionizing states taking into account the broadening effects due to both plasma electrons and ions, as well as natural and Doppler broadening [71]. Ion microfield distribution functions were computed with the APEX model assuming equal electron and ion temperatures [72]. Also, since deuterium ions are the dominant perturbing ion in the argon-doped implosion core plasmas, ion dynamics effects were also considered in the Stark line broadening calculation according to the formalism discussed in [73]. A detailed analysis of the theoretical spectrum in Fig. 5 illustrates some of the outstanding issues. If we consider only Ar *K*-shell line emission the synthetic spectrum (see Fig. 5 theory (a)), drops significantly at high photon energies and it cannot reach the overall intensity level in the measured spectrum. If the continuum emission produced by the radiative recombination from the H-like ground state into He-like ground state is included, the intensity level increases. The addition of the bound-free emission from nl H-like excited states to 1s*nl* He-like excited states (up to $n=4$) (see Fig. 5 theory (c)) causes an additional small increase of intensity. Finally, when the bound-free emission from fully-stripped into H-like ground state is included (see Fig. 5 theory (d)) the model produces better overall agreement with the observed intensity. The temperature and density extracted from the best fit were $T_e=1410$ eV and $N_e=2.3\times10^{24}$ cm^{-3}. If we restrict the comparison to the narrower energy interval from 3500 to 4000 eV and do not include the bound-free emission, then the extracted conditions are $T_e=1470$ eV and $N_e=2.4\times10^{24}$ cm^{-3}. A more detailed study of this theoretical analysis can be found in [74].

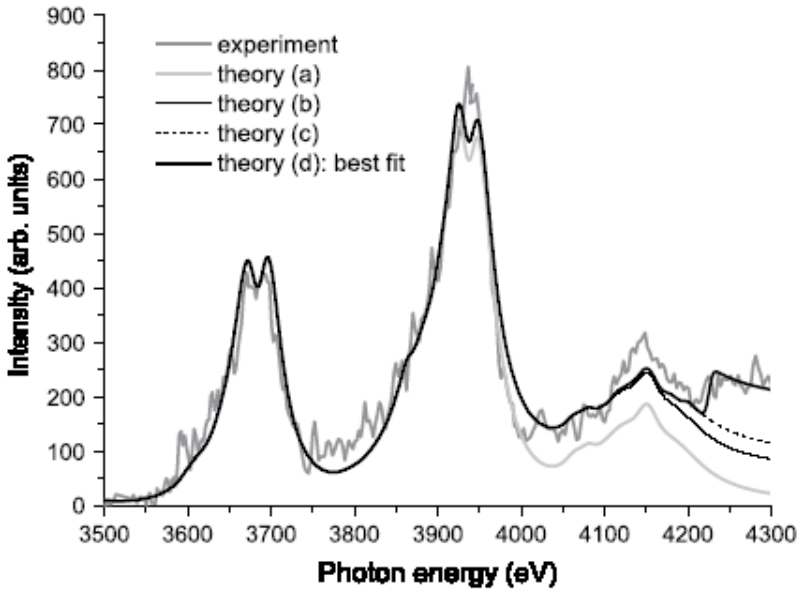

Figure 5: Comparison between a time-resolved spectrum for OMEGA shot 49956 and theoretical spectra including a different number of radiative recombination emissions: (a) only radiation emitted from Ar *K*-shell lines has been considered; (b) including the bound-free emission from H-like ground state into He-like ground state; (c) including also bound-free emission from *nl* H-like excited states into 1s*nl* He-like excited states; (d) further including recombination from fully-stripped to H-like ground state, i.e. full calculation. Figure extracted from [74].

3.3 Optically thick non-homogeneous plasmas

For this item, we have determined the average ionization in a non-homogeneous aluminum plasma with planar geometry. We carried out the calculations over two different pairs of density and temperature profiles, which were provided by hydrodynamic simulations with the 2D-hydrodynamic code ARWEN [75] of the aluminum experiments carried out at LULI [68] commented in the previous subsection. One of the cases presents a strong gradient in temperature and density (see Fig. 6, left) while the other one shows a smooth variation (see Fig. 7, left). The calculations were done using an atomic database which includes only 325 levels, for ions from neutral to full stripped aluminum, since our interest was focused on the effects of including the radiative transfer model. To show the suitability of the proposed model, we have carried out three different types of calculations: no-radiation, i.e. we consider complete uncoupled cells and we also consider that they are thin, so any absorption effect is not included in the model; no-coupling, i.e. we consider complete uncoupled cells but we take into account only the probability that one photon emitted in a given cell is absorbed in the same cell, and coupling, i.e. with the cells coupled as it was explained previously. In Fig. 6, we have compared the effect of the three approaches in the average ionization. The length of the plasma is equal to $200\mu m$, $z=0$ denotes the position of the plasma crater after the shot and z rises as we move away

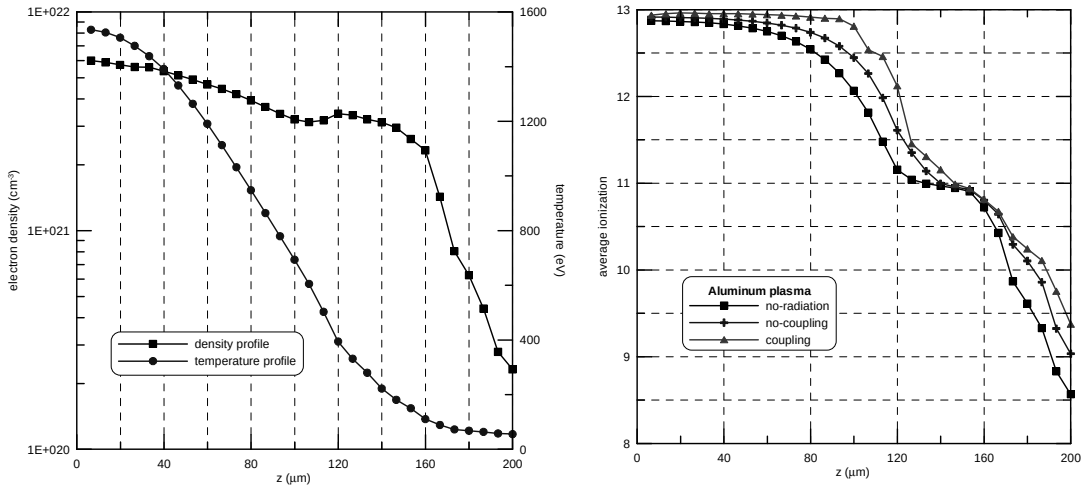

Figure 6: Spatial electron density and temperature profiles for first proposed case (on the left). The corresponding spatial average ionization distribution for the three types of mentioned calculations (on the right).

from the crater. First of all, we observe that the main effect of the self-absorption is to increase the average ionization, which is expected. For values of z lower than $20\mu m$ the average ionization provided by the three models are quite similar. In this region, the plasma is highly ionized and the depth in the plasma is small and both factors produce that the opacity effects to be small. The differences increase as z does but it is found a region around $140\mu m$ where the three models predict almost the same average ionization, which is 11. This feature is due to the relevant abundance of He-like ion in the range $120-160\mu m$ in the calculation without including opacity effects. For higher values of z, the plasma ionization decreases and the opacity effects become larger. Moreover, the length of the plasma is also bigger which implies more differences between no-coupling and coupling calculations.

In Fig. 7 $z=160\mu m$ denotes the location of the plasma crater after the shot and z decreases as we move away from the crater. As we go deeper in the plasma, the differences in the average ionization provided by the three approaches increase according to the above explained. We have also compared our results with a calculation performed using the LTNEP code [76], which solves the time independent 1D equation transfer self-consistently with rate equations. From the figure, it is observed an excellent agreement between our model and LTNEP code.

4 Conclusions

In this work we have presented ABAKO/RAPCAL, a versatile CR model designed to determine the population distribution of atomic levels and radiative properties of steady-state NLTE plasmas. During its development, a compromise between accuracy and com-

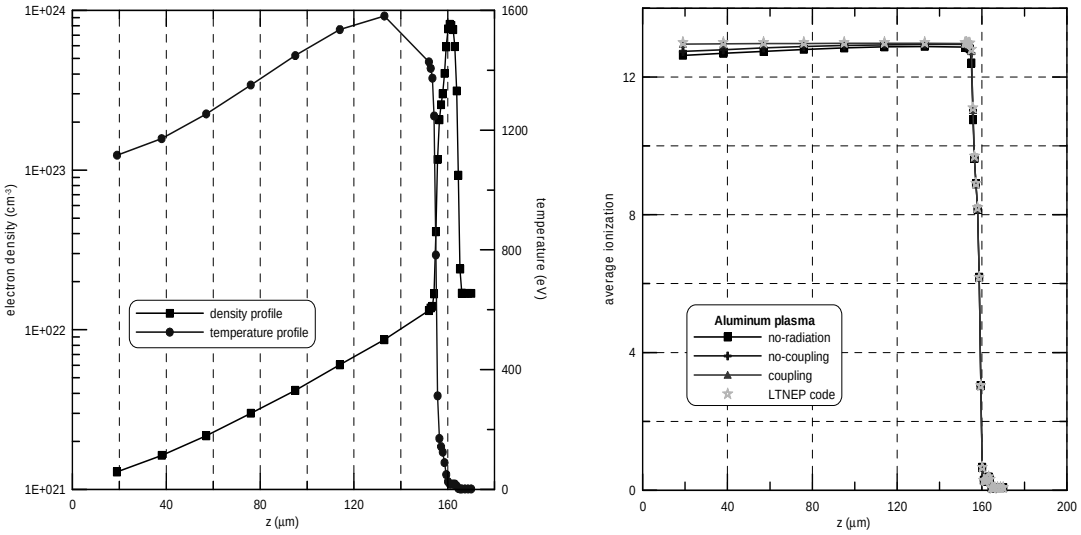

Figure 7: Spatial electron density and temperature profiles with a strong gradient (on the left). The corresponding spatial average ionization distribution for the three types of mentioned calculations (on the right).

putational cost was achieved. Hence, ABAKO/RAPCAL incorporates a set of simple analytical models, which yield a substantial saving of computational requirements, but providing satisfactory results in relation to those obtained from more elaborate codes and experimental data. Self-absorption effects in uniform plasmas are taken into account via escape factors for the three basic geometries—plane, cylindrical and spherical. The self-absorption in non-homogeneous plasmas are also modeled, for planar geometry only, using a new technique for the line-photon transport relied on the definition of zone-to-zone radiative coupling coefficients. Furthermore, since the determination of level population distributions often involve very large sparse CR matrices, iterative methods are used to perform the matrix inversion because they typically require less memory and can yield an approximation to the solution significantly faster than a direct method. Furthermore, the calculation of the atomic processes and the resolution of the CR matrix have been parallelized with the consequent reduction of computing time. We have also presented some results and comparisons for low and high-Z, optically thin and thick (homogeneous and non-homogeneous) plasmas. In general, the results obtained with ABAKO/RAPCAL agree well with those given by other codes or with experimental measurements. Therefore, ABAKO/RAPCAL results a versatile CR model which can be applied to low-to-high Z ions with a variety of laboratory plasma conditions: CE, LTE or NLTE, optically thin or thick plasmas.

On the other hand, since ABAKO/RAPCAL package includes some simple analytical models, it has several limitations. Thus, its application for very high density plasmas is limited by the Stewart and Pyatt model used for the continuum lowering. Besides, some of the analytical rate coefficients, such as collisional excitation and ionization ones, may not be accurate for cold plasmas, which limits the validity of the package to plasma

temperatures greater than 1 eV. We have also observed that the proposed formalism to calculate the autoionization and electron capture rate coefficients should be revised for high-Z plasmas at high temperatures, since it leads to anomalous high values of the average ionization. The rates should be also improved for low density spectroscopy where the very high spectral resolution allows the fine structure lines to be observed. In addition, we have not probed the validity of ABAKO/RAPCAL to perform spectroscopic diagnostics to more complex ions which involve L-shell or M-shell spectra.

For these reasons, ABAKO/RAPCAL is still under development. Nowadays, we are working on the parallelization of the module devoted to the calculation of the radiative properties. We are also designing a web user interface to provide remote execution. Furthermore, we are developing a method based on genetic algorithms to improve our method to perform spectroscopic diagnostics. Other improvements already underway are the extension to non-Maxwellian electron distributions and the explicit consideration of atomic processes driven by an external radiation field and modeling of time-dependent population kinetics. Finally, we are also concerned with the improvement of the rate coefficients. We are aware that recently published works will allow us an updating and improvement of the analytic expressions used to compute the rate coefficients.

Acknowledgments

This work has been supported by the Research Project of the Spanish Government (ENE2008-06668-C02-02/FTN) and also by the *Keep in touch* Project of the European Union.

References

[1] A. Bar-Shalom, J. Oreg and M. Klapisch, Recent developments in the SCROLL model, J. Quant. Spectrosc. Radiat. Transfer, 65 (2000), 43-55.
[2] O. Peyrusse, A superconfiguration model for broadband spectroscopy of non-LTE plasmas, J. Phys. B: At. Mol. Opt. Phys., 33 (2000), 4303-4321.
[3] A. Bar-Shalom, M. Klapisch and J. Oreg, HULLAC, an integrated computer package for atomic processes in plasmas, J. Quant. Spectrosc. Radiat. Transfer, 77 (2001), 169-188.
[4] Yu. V. Ralchenko and Y. Maron, Accelerated recombination due to resonant deexcitation of metastable states,J. Quant. Spectrosc. Radiat. Transfer, 71 (2001), 609-621.
[5] G. Faussurier, C. Blancard and E. Berthier, Nonlocal thermodynamic equilibrium self-consistent average-atom for plasma physics, Phys. Rev. E, 63 (2001), 026401.
[6] S.B. Hansen, Development and application of L-shell spectroscopic modeling for plasma diagnostics, Ph.D. Thesis, University of Nevada, (2003).
[7] J. Bauche, C. Bauche-Arnoult and K.B. Fournier, Model for computing superconfiguration temperatures in non-local-thermodynamic-equilibrium hot plasmas, Phys. Rev. E, 69 (2004), 026403.

[8] H. K. Chung, M. H. Chen, W. L. Morgan, Y. Ralchenko and R. W. Lee, FLYCHK: Generalized population kinetics and spectral model for rapid spectroscopic analysis for all elements, High Energy Density Phys., 1 (2005), 3-12.
[9] C.J. Fontes, J. Colgan, H.L. Zhang and J. Abdallah Jr., Large-scale kinetics modeling of non-LTE plasmas, J. Quant. Spectrosc. Radiat. Transfer, 99 (2006), 175-185.
[10] J. Q. Pang, Z. Q. Wu and J. Yan, Emissivity calculations under DCA-UTA approximation for NLTE plasmas, Commun, Comput. Phys., 2 (2007), 1085-1094.
[11] D. R. Bates, A. E. Kingston and R.W. P.McWirther, Recombination between electrons and atomic ions. I. Optically thin plasmas, Proc. R. Soc. London, Ser. A, 267 (1962),297-312.
[12] R. W. P. McWhirther, Data needs, priorities and accuracies for plasma spectroscopy, Phys. Rep., 37 (1978), 165-209.
[13] S. Mazevet and J. Abdallah Jr., Mixed UTA and detailed line treatment for mid-Z opacity and spectral calculations, J. Phys. B: At. Mol. Opt. Phys., 39 (2006), 3419-3429.
[14] O. Peyrusse, Complex atom physics and radiative properties of hot dense plasmas, Nucl. Fusion, 44 (2004), S202-S207.
[15] M. Poirier, On various validity criteria for the configuration average in collisional-radiative codes, J. Phys. B: At. Mol. Opt. Phys., 41 (2008), 025701.
[16] A. Bar-Shalom, J. Oreg and M. Klapisch, Non-lte superconfiguration collisional radiative model, J. Quant. Spectrosc. Radiat. Transfer, 58 (1997), 427-439.
[17] J. Bauche, C. Bauche-Arnoult and M. Klapisch, Transition arrays in the spectra of ionized ions, Adv. At. Mol. Phys., 23 (1987), 131-195.
[18] J. Bauche, C. Bauche-Arnoult and M. Klapisch, Breakdown of jj coupling in spin-orbit-split atomic transition arrays, J. Phys. B: At. Mol. Opt. Phys., 24 (1991), 1-11.
[19] A. Bar-Shalom, J. Oreg, W. H. Goldstein, D. Shvarts, A. Zigler, Super-transition-arrays: a model for the spectral analysis of hot dense plasmas, Phys. Rev. A, 40 (1989), 3183-3193.
[20] S. Hansen, J. Bauche, C. Bauche-Arnoult and M. F. Gu, Hybrid atomic models for spectroscopic plasma diagnostics, High Energy Density Phys., 3 (2007), 109-114.
[21] J. Abdallah Jr. and M. E. Sherrill, The reduced detailed configuration accounted (RDCA) model for NLTE plasma calculations, High Energy Density Phys., 4 (2008), 124-130.
[22] D. Mihalas, Stellar Atmospheres, W. H. Freeman and Company, 1970.
[23] D. Mostacci, L. M. Montierth, J. P. Dinguirard and R. L. Morse, X-ray line emission from laser-produced spherical plasma flows, Phys. Fluids B, 1 (1989), 2106-2120.
[24] D. C. Eder and H. A. Scott, The calculation of line transfer in expanding media, J. Quant. Spectrosc. Radiat. Transfer, 45 (1991), 189-204.
[25] O. Peyrusse, A model for the simulation of nonequilibrium line transfer in laboratory plasmas, Phys. Fluids B, 4 (1992), 2007-2017.
[26] I. Hubeny and T. Lanz, Non-LTE line-blanketed model atmospheres of hot stars. I. Hybrid complete linearization/accelerated lambda iteration method, Astrophys. J., 439 (1995), 875-904.
[27] F. E. Irons, The escape factor in plasma spectroscopy–I. The escape factor defined and evaluated, J. Quant. Spectrosc. Radiat. Transfer, 22 (1979), 1-20.
[28] F. E. Irons, The escape factor in plasma spectroscopy–II. The case of radiative decay, J. Quant. Spectrosc. Radiat. Transfer, 22 (1979), 21-36.
[29] F. E. Irons, The escape factor in plasma spectroscopy–III. Two cases studies, J. Quant. Spectrosc. Radiat. Transfer, 22 (1979), 37-44.
[30] J. P. Apruzese, Direct solution of the equation of transfer using frequency- and angle-averaged photon-escape probabilities for spherical and cylindrical geometries, J. Quant.

Spectrosc. Radiat. Transfer, 25 (1980), 419-425.
[31] J. P. Apruzese, J. Davis, D. Duston and K. G. Whitney, A direct solution of the equation of transfer using frequency- and angle-averaged photon escape probabilities, with application to a multistage, multilevel aluminum plasma, J. Quant. Spectrosc. Radiat. Transfer, 23 (1980), 479-487.
[32] J. P. Apruzese, An analytical Voigt profile escape probability approximation, J. Quant. Spectrosc. Radiat. Transfer, 34 (1985), 447-452.
[33] C. Bowen, R. W. Lee and Yu. Ralchenko, Comparing plasma population kinetics codes: Review of the NLTE-3 Kinetics Workshop, J. Quant. Spectrosc. Radiat. Transfer, 99 (2006), 102-119.
[34] J. G. Rubiano, R. Florido, C. Bowen, R. W. Lee, Y. Ralchenko, Review of the 4th NLTE code comparison workshop, High Energy Density Phys., 3 (2007), 225-232.
[35] C. J. Fontes, J. Abdallah Jr., C. Bowen, R. W. Lee, Y. Ralchenko, Review of the NLTE-5 kinetics workshop, High Energy Density Phys., 5 (2009), 15-22.
[36] R. Florido, R. Rodriguez, J. M. Gil, J. G. Rubiano, P. Martel, D. Suarez, M. Mendoza, E. Minguez, ABAKO: a new code for population kinetics and radiative properties of plasmas under NLTE conditions, J. Phys. Conf. Ser., 112 (2008), 042008.
[37] R. Florido, R. Rodriguez, J. M. Gil, J. G. Rubiano, P. Martel, E. Minguez and R. C. Mancini, Modeling of population kinetics of plasmas that are not in local thermodynamic equilibrium, using a versatile collisional-radiative model based on analytical rates, Phys. Rev. E, 80 (2009), 056402.
[38] R. Rodriguez, R. Florido, J. M. Gil, J. G. Rubiano, P. Martel and E. Minguez, Rapcal code: a computational package to compute radiative properties for optically thin and thick low and high-Z plasmas in a wide range of density and temperature, Laser Part. Beams, 26 (2008), 433-448.
[39] P. Martel, J. G. Rubiano, J. M. Gil, L. Doreste and E. Minguez, Analytical expressions for the n-order momenta of charge distribution for ions, J. Quant. Spectrosc. Radiat. Transfer, 60 (1998), 623-633.
[40] R. Rodriguez, J. G. Rubiano, J. M. Gil, P. Martel and E. Minguez, Development of an analytical potential to include excited configurations, J. Quant. Spectrosc. Radiat. Transfer, 75 (2002), 723-739.
[41] J. M. Gil, P. Martel, E. Minguez, J.G. Rubiano, R. Rodrguez and F. H. Ruano, An effective analytical potential including plasma effects, J. Quant. Spectrosc. Radiat. Transfer, 75 (2002), 539-557.
[42] R. Rodriguez, J. M. Gil and R. Florido, Screening effects on the atomic magnitudes of non-hydrogenic ions in strongly coupled plasmas, Phys. Script., 76 (2007), 418-427.
[43] J. M. Gil, R. Rodriguez, R. Florido, J. G. Rubiano, P. Martel and E. Minguez, Determination of corona, LTE and NLTE regimes of optically thin carbon plasmas, Laser Part. Beams, 26 (2008), 21-31.
[44] M. F. Gu, Indirect x-ray line-formation processes in iron l-shell ions, Astrophys. J. 582 (2003), 1241-1250.
[45] J. C. Stewart and K. D. Pyatt, Lowering of ionization potentials in plasmas, Astrophys. J., 144 (1966), 1203-1211.
[46] R. M. More, Atomic physics in inertial confinement fusion, Technical Report UCRL-84991, Lawrence Livermore National Laboratory, 1981.
[47] M. K. Chung, M. H. Chen and R. W. Lee, Extension of atomic configuration sets of the Non-LTE model in the application to the Kα diagnostics of hot dense matter, High Energy Density

Phys., 3 (2007), 57-64.
[48] W. Lotz, Electron-impact ionization cross sections and ionization coefficients for atoms and ions from hydrogen to calcium, Z. Phys. 216 (1968), 241-247.
[49] H. V. Van Regemorter, Rate of collisional excitation in stellar atmospheres, Astrophys. J. 136 (1962), 906-915.
[50] H. A. Kramers, On the theory of X-ray absorption and of the continuous X-ray spectrum, Philos. Mag. 46 (1923), 836-871.
[51] H. R. Griem, Principles of plasma spectroscopy, Cambridge University Press, 1997.
[52] R. C. Mancini, R. F. Joyce, and C. F. Hooper Jr., Escape factors for Stark-broadened line profiles, J. Phys. B: At. Mol. Phys., 20 (1987), 2975-2987.
[53] M. S. Dimitrijevic and N. Konjevic, Simple estimates for Stark-broadening of ion lines in stellar plasmas, Astron. & Astrophys., 172 (1987), 345-349.
[54] R. Florido, –ABAKO– Un modelo para el estudio de la cinetica de poblaciones y propiedades radiativas de plasmas bajo condiciones de no-equilibrio, Ph. D. Thesis, Universidad de Las Palmas de Gran Canaria, 2007.
[55] R. C. Mancini (private communication).
[56] S.J. Rose, Calculations of the radiative opacity of laser-produced plasmas, J. Phys. B: At. Mol. Opt. Phys., 25 (1992), 1667-1681.
[57] Y. Saad, Iterative methods for sparse linear systems, PWS Publishing Company, 1995.
[58] CXML Team, Compaq Extended Math Library Reference Guide, Compaq Computer Corporation, 1999.
[59] I. Foster, Defining and building parallel programs, Addison-Wesley, 1995.
[60] G. Burns, R. Daoud and J. Vaigl, LAM: an open cluster environment for MPI, Proceedings of Supercomputing Symposium, (1994), 379-386.
[61] W. Gropp, E. Lusk and R. Thakur, MPI-2: Advanced features for the MPI, MIT Press, 1999.
[62] J. Colgan, C. J. Fontes and J. Abdallah Jr., Collisional-radiatives calculation of carbon plasmas, High Energy Density Phys. 2 (2006),90-96.
[63] H.K. Chung, K.B. Fournier and R.W. Lee, Non-LTE kinetics modelling of krypton ions: Calculation of radiative cooling coefficients, High Energy Density Phys. 2 (2006), 7-15.
[64] M. Klapisch, A program for atomic wavefunction computations by the parametric potential method, Comput. Phys. Commun. 2 (1971), 239-260.
[65] J. Oreg, W.H. Goldstein and M. Klapisch, Autoinization and radiationless electron capture in complex spectra, Phys. Rev. A. 44 (1991), 1750-1758.
[66] A. Bar-Shalom, M. Klapisch and J. Oreg, Electron collision excitations in complex spectra of ionized heavy atoms, Phys. Rev. A 38 (1988), 1773-1784.
[67] K.B. Fournier, M.J. May, D. Pacella, M. Finkenthel, B.C. Gregory and W.H. Goldstein, Calculation of the radiative cooling coefficient for krypton in a low density plasma, Nucl. Fusion 40 (2000), 847-863.
[68] R. Schott, F. Philippe, P. Angelo, E. Dufour, A. Poquerusse, E. Leboucher-Dalimier, P. Sauvan, P. Velarde, F. Ogando, E. Minguez, J. M. Gil, J. G. Rubiano, R. Rodriguez, P. Martel and R. Mancini, Access to spectrally resolved ultra-dense hot low Z emissivities and opacities, 16th International Conference on Spectral Line Shapes, American Institute of Physics (2002), 340-351.
[69] R. Florido, T. Nagayama, R.C. Mancini, R. Tommasini, J.A. Delettrez, S.P. Regan, V.A. Smalyuk, R. Rodriguez, J.M. Gil, Analysis of time-resolved argon line spectra from OMEGA direct-drive implosions, Rev. Sci. Instrum. 79 (2008), 10E310.
[70] T.J. Burris-Mog, R.C. Mancini, J.E. Bailey, G.A. Chandler, G. Rochau, G. Dunham, P.W. Lake,

K. Peterson, S.A. Slutz, T.A. Mehlhorn, I.E. Golovkin, J.J. MacFarlane, Line broadening analysis of implosion core conditions at Z using argon K-shell spectroscopy, J. Quant. Spectrosc. Radiat. Transf. 99 (2006), 120-130.

[71] R.C. Mancini, D.P. Kilcrease, L.A. Woltz, C.F. Hooper Jr., Calculational aspects of the Stark line broadening of multielectron ions in plasmas, Comput. Phys. Commun. 63 (1991), 314-322.

[72] C.A. Iglesias, H.E. DeWitt, J.L. Lebowitz, D. MacGowan, W.B. Hubbard, Low-frequency electric microfield distributions in plasmas, Phys. Rev. A 31 (1985), 1698-1702.

[73] D.A. Haynes Jr., D.T. Garber, C.F. Hooper Jr., R.C. Mancini, Y.T. Lee, D.K. Bradley, J. Delettrez, R. Epstein, P.A. Jaanimagi, Effects of ion dynamics and opacity on Stark-broadened argon line profiles, Phys. Rev. E 53 (1996), 1042-1050.

[74] R. Florido, R.C. Mancini, T. Nagayama, R. Tommasini, J.A. Delettrez, S.P. Regan, V.A. Smalyuk, R. Rodriguez, J.M. Gil, Argon K-shell and bound-free emission from OMEGA direct-drive implosion core, High Energy Density Phys. (2009), doi:10.1016/j.hedp.2009.06.011.

[75] F. Ogando and P. Velarde, Development of a radiation transport fluid dynamic code using AM3 scheme, J. Quant. Spectrosc. Radiat. Transfer, 71 (2001), 541-550.

[76] I. Hubeny and T. Lanz, Accelerated complete-linearization method for calculating NLTE model stellar atmospheres, Astron. & Astrophys., 262 (1992), 501-514.